Wear 452–453 (2020) 203289

Contents lists available at ScienceDirect

Wear

journal homepage: http://www.elsevier.com/locate/wear

Investigation of single asperity wear at the microscale in an austenitic steel

Wenzhen Xia [a,*], Gerhard Dehm [a], Steffen Brinckmann [a,b,**]

[a] Department of Structure and Nano-/Micromechanics of Materials, Max-Planck-Institut für Eisenforschung GmbH, Düsseldorf, 40237, Germany
[b] Microstructure and Properties of Materials (IEK-2), Forschungszentrum Jülich, 52428, Germany

ARTICLE INFO

Keywords:
Single asperity
Wear
Plasticity
Pile-up
Slip-step

ABSTRACT

Engineering surfaces consist of microasperities, which result in plasticity during the run-in of the tribological system. A fundamental insight of the plastic flow during single asperity wear at the microscale is required to thoroughly understand tribology induced microstructure at the macroscale and to tailor future metal surfaces. In this work, we indent and wear {001}-, {101}- and {111}-grains in an austenite stainless steel. The transition from indentation to ploughing and the evolution of plasticity during ploughing is addressed. We find that slip-step and pile-up evolution during the indentation segment of the wear experiment influence the plasticity during the ploughing segment that follows upon the indentation. We conclude that the pile-up evolution dominates the development of the friction force during ploughing at the microscale.

1. Introduction

Tribology is the study of interacting surfaces during relative motion and it plays an important role in the modern world's energy consumption [1,2]. Due to the complex interaction of the tribological processes (e.g. stress-state, plasticity, microstructure evolution, chemistry), it is challenging to decipher relations between the microstructure and tribological properties, even though tribology has been studied for centuries. For instance, the properties of tribological metallic contacts are largely determined by the plastic deformation using millimeter asperities [3]. Lately, the evolution of subsurface dislocation lines was observed [4,5], although the dislocation mechanisms (i.e. plastic mechanisms) are still at large during tribology. Due to the advance in high-resolution characterization and micromachining, it is possible to separate the tribological processes. Single asperity wear, i.e. nano/micro scratch testing, has become a useful technique for studying the ploughing-induced plasticity and characterizing the tribological properties of materials at the nano/microscale [6–13].

Single asperity wear aims also at measuring the friction force or coefficient of friction depending on the material properties and the contact topology. Amontons and Coulomb proposed the macroscopic friction law $F_{fric} = \mu F_n$, where F_{fric} is the lateral friction force, F_n is the normal force and μ is the friction coefficient. Bowden and Tabor [14] put forward that the surface consists of many microasperities and that friction consists of two processes: adhesion and abrasion. Based on the Bowden and Tabor model, Moore [15], Lafaye et al. [16–18], Goddard and Wilman [19], etc. developed analytical models describing friction for different contact topologies and material indentation hardness. The authors did not account for the pile-up on the backside of the asperity.

The microstructure and mechanical properties affect the general concepts of tribology. Due to anisotropy, the plasticity depends on the crystal orientation and wear direction during single asperity wear. The pile-up and dislocation evolution are the results of dislocation glide on [110]{111} slip systems during wear in the face-centered cubic (FCC) metals, in which dislocation mediated plasticity dominates [10,20]. Therefore, non-symmetric plasticity occurs during ploughing [10] even under symmetrical loading (e.g. spherical tip). The anisotropy is amplified by using non-symmetric asperities, e.g. Berkovich tip [11,21]. Simulations using different frameworks and length scales have been performed to unravel ploughing and develop an understanding of the mechanisms:

1) Finite element simulation (FEM) at the macroscale: FEM studies [22,23] have used isotropic constitutive laws and provided useful insights into ploughing, i.e. surface topography and pile-up evolution. These numerical results were compared to the experimental observation. However, the crystallographic orientation was not addressed with that method.
2) Crystal plasticity based finite element simulations (CP-FEM) at the mesoscale: CP-FEM accounts for the anisotropy of elastic-plastic

* Corresponding author.
** Corresponding author.
E-mail addresses: w.xia@mpie.de (W. Xia), s.brinckmann@fz-juelich.de (S. Brinckmann).

https://doi.org/10.1016/j.wear.2020.203289
Received 12 December 2019; Received in revised form 1 April 2020; Accepted 2 April 2020
Available online 9 April 2020

crystalline materials and simulates the slip-plane based plasticity [24]. Wang et al. [21] investigated and quantified the plasticity on crystallographic orientations during ploughing with a Berkovich tip. The results show that the anisotropic characteristics are determined by the crystallographic orientation and the extrinsic discrete stress distribution induced by tip geometry. However, CP-FEM is a continuum approach that cannot predict discrete dislocations on the inherently discrete slip-steps [4,25].

3) Discrete dislocation dynamics (DDD) at the microscale studies discrete dislocation motion, multiplication, interactions and dislocation network evolution in response to external loading. Gagel et al. [25] performed a 3D-DDD simulation of a sliding spherical tip on an FCC crystal. The results show that the dislocations are partly transported by the tip along the sliding direction. They also identified the distance of dislocation motion along sliding direction depending on the slip system orientation. However, the pile-up and abrasion development were not considered in this study.
4) Molecular dynamics (MD) at the nanoscale: DDD simulations generally use phenomenological laws to prescribe dislocation nucleation in the perfect crystal, while MD simulations intrinsically handle the physics of dislocations, including dislocation nucleation, as well as the pile-up formation. Multiple MD studies have been conducted for nanoscale scratching of different metals, e.g. silver [26], aluminum [27,28], copper [29,30], high entropy alloy [31,32], etc. Their results showed in details the developments of the scratch groove, pile-up around the groove as well as the plasticity underneath the groove. Despite the increase in understanding of tribology at the nanoscale, MD simulations are very limited by the small length, short time and very large strain rate scale.

Other researchers have furthered the understanding of tribology. Chamani and Ayatollahi [11] showed the importance of the front pile-up on the coefficient of friction (COF) using edge-forward and side-forward directions of a Berkovich tip. Brinckmann et al. [9,10] performed a microasperity wear experiment on a FCC metal and observed that three domains occur with increasing normal force: elastic-, plastic ploughing and wear particle-dominated tribology. In the elastic regime, Ye et al. [33] found that an increase in the normal load results in a COF decrease. In the plastic regime, the authors observed a constant COF for different normal forces in a body-centered cubic (BCC) high-entropy alloy. Multiple researchers [9–11,21,34] observed the same trend of the friction force: the friction force increases until it reaches a steady-state value with increasing wear distance at constant load.[1] Although frequently observed, the underlying mechanism of the friction force increase towards the steady state value was not addressed in those studies.

This experimental study aims at understanding the plastic flow and change in friction force during single asperity wear tests on an austenitic steel. We conduct the indentation and the scratching with varying lengths in three coarse grains with different orientations. For the different grain orientations we discuss: 1) how indentation influences the subsequent ploughing segment; 2) the differences in plasticity between indentation and wear; 3) the evolution of plasticity towards the steady-state topology and 4) the correlation of plasticity and the friction force during ploughing.

2. Experimental procedure

The as-received Fe-25Cr-20Ni austenitic stainless steel was annealed at 1200 °C for one week in order to obtain a coarse single phase FCC microstructure, which allows conducting a series of wear tests in an individual grain without grain boundary interference. The sample surface was wet ground, polished with diamond paste and then with colloidal silica (OPS). Afterwards, the sample was slightly etched with a solution of V_2A (10 ml HNO_3, 0.30 ml Vogels pickling inhibitor, 100 ml HC1 and 100 ml H_2O) to remove any deformation layer produced by the previous preparation steps. Finally, 30 min OPS polishing was applied to remove the chemical reaction layer of the etching process. After sample preparation, Electron Backscatter Diffraction (EBSD) was conducted to determine the grain orientation. Three large grains with normal orientations close to {001}, {110} and {111} were identified for microscale testing. Their precise orientations were $(5\ \bar{6}\ 25)$, $(2\ \overline{13}\ 13)$ and $(18\ 20\ 19)$, respectively.

The indentation and wear tests were conducted in an Agilent/Keysight/KLA G200 nanoindenter with a spherical diamond tip (nominal radius = 5 μm). The normal force (40 mN) and loading/unloading rate (0.5 mN/s) were applied for both tests (indentation and wear). Wear tracks of varying lengths (2, 4, 6, 8, 10 and 20 μm) and a tangential velocity of 1 μm/s were used to follow the plasticity evolution in the three grains. An additional distance (10%) with a minimal normal force (0.15 mN) was added to the front and end of the wear track to determine the sample tilt. After deformation, the sample was inspected in a ZEISS Merlin field emission SEM with the secondary electron (SE) detector for the slip-step pattern and the Backscatter electron detector (BSD) for the Electron Channeling Contrast Images (ECCI) of the dislocation structures. A confocal microscopy (μsurf, NanoFocus Messtechnik GmbH, Germany) was used to quantify the pile-up heights.

In this study, the slip steps on the surface were identified by EBSD and ECCI. In order to analyze the slip steps, we distinct slip-planes and the plasticity on these planes based on the plane inclination: positively inclined and negatively inclined planes. Initially, these are the terms for slip-step distinction in indentation [35]: positively inclined slip plane is a plane on which the dislocations move from the area of highest shear stresses underneath the indenter to the surface; the dislocations travel on the negatively inclined slip planes from the outside perimeter to the surface and closer to the indenter during indentation (see Fig. 1).

3. Results

In this section, we firstly show the plasticity evolution, i.e. slip-step and pile-up developments, from indentation to short ploughing (2, 4, 6, 8 and 10 μm) in the {111}, {101} and {001} grains. Afterwards, the morphologies of the slip-step and the pile-up in the long ploughing (20 μm) are presented in detail. Finally, we illustrate the change in the fiction force during ploughing.

3.1. Transition from indentation to short wear distance

3.1.1. Slip-step morphology

The SEM images of the {111}, {101} and {001} grains after the indentation and after the short ploughing (2 μm length) are shown in Fig. 2. In these three grain orientations, the area in the front of the

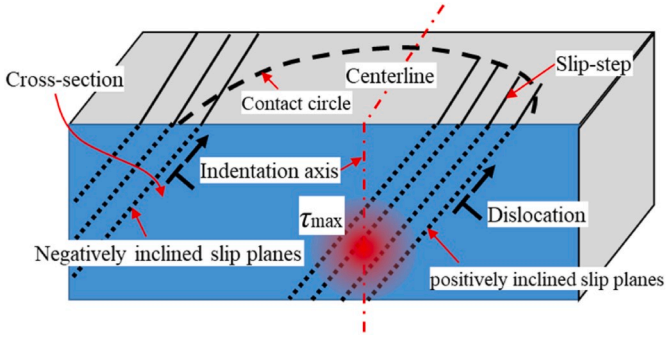

Fig. 1. Schematic sketch of positively and negatively inclined planes in indentation.

[1] It should be noted that these discussed friction forces are each dynamic friction forces and do not relate to the static friction – dynamic friction transition.

indenter during the indentation and the ploughing can be divided into three domains: I, II and III. Slip activity only occurs in the domains I and III while no slip-steps are observed in domain II, although it is in between domains I and III. The slip-step patterns in domains I and III widen during ploughing, compared to the width during indentation but keep geometric similarity. This similarity of slip-step patterns confirms that the indentation and ploughing induced plasticity are grain orientation dependence. On the one hand, the centers of the slip-step patterns in the domains I and III of the indentation and the ploughing locate in the similar direction with rotation angles, with respect to the indenter center. One the other hand, the slip-step patterns are asymmetric on both sides of the wear track.

In the {111} grain, both slip-step patterns consist of slip-steps on P(1 1 $\bar{1}$), P(1 $\bar{1}$ $\bar{1}$) and N(1 $\bar{1}$ 1) planes in the domains I after indentation and ploughing, as shown in Fig. 2(b) and (c). The domains I locates closer to the front of the indenter. During ploughing, slip on P(1 1 $\bar{1}$), N(1 $\bar{1}$ 1) and P(1 $\bar{1}$ $\bar{1}$) increases more severely in domain I. In domains III, during indentations the negatively inclined N(1 1 $\bar{1}$) slip-planes are activated by pile-up formation, which is produced by slip on the positively inclined P(1 $\bar{1}$ 1), P(1 $\bar{1}$ $\bar{1}$) slip-planes during the initial stage [35]. However, during ploughing, the N(1 1 $\bar{1}$) slip plane becomes more dominant; this slip system mainly grows forward in the direction of ploughing, see Fig. 2(b) and (c).

In the {101} grain, it should be noted that the (1 $\bar{1}$ $\bar{1}$) and (1 1 1) planes are almost perpendicular to the surface (neither positive nor negative). More slip occurs in the domains I, i.e. in the ploughing direction and to the left side, during the indentation and the ploughing. Two main slip systems, P(1 1 $\bar{1}$) and (1 $\bar{1}$ $\bar{1}$), are active, which facilitate the plasticity flow away from the imprints. Some slip-steps on the (1 1 1) planes are observed close to the imprint in the domain I during the indentation and the ploughing. In the domains III, minor slip activity occurs on the N(1 1 $\bar{1}$) planes during the indentation while it becomes a dominant slip system during ploughing, resulting in forward growth of the corresponding slip-steps in the ploughing direction, see Fig. 2(d) and (f). It is similar to the N(1 1 $\bar{1}$) planes in the domain III in the {111} grain.

In the {001} grain, the same mechanisms are observed as in the previously discussed grains: spread of slip-steps in the domains I and III; the domain II remains few slip steps and separates the domains I and III. Specially, the slip-step lines on the (1 $\bar{1}$ 1) and (1 $\bar{1}$ $\bar{1}$) are almost parallel in this grain. The further details on slip step activity, in the P(1 $\bar{1}$ $\bar{1}$) or N(1 $\bar{1}$ 1) planes, in the domain I will be identified from ECCI and discussed subsequently.

3.1.2. Dislocation morphology

Fig. 3 shows the dislocation morphology after indentation and after short ploughing in the {101} grain. The dislocations on the (1 1 $\bar{1}$) plane are perfect dislocations in the domains I and III after indentation, as shown in Fig. 3(a) and (b). These ECCI images show the positive inclination in the domain I: dislocation lines are toward the indent; and the negative inclination in the domain III: the dislocation trace lines are away from the imprint. After ploughing, the dislocations on the (1 1 $\bar{1}$) plane are dissociated into partial dislocations in the domain III (Fig. 3 (d)), However, the dislocations in the domain I – on the left-hand side – remain as perfect dislocations (Fig. 3(c)).

Fig. 4 shows the ECCI images after indention and 2 μm ploughing in the {001} grain. We focus on determining on which plane the slip steps are in the domains I: P(1 $\bar{1}$ $\bar{1}$) or N(1 $\bar{1}$ 1) planes? During the indentation, it is on the N(1 $\bar{1}$ 1) plane, as shown in Fig. 4(a), and this secondary-plasticity is the result of pile-up formation that was produced by the P(1 1 1) and P(1 1 $\bar{1}$) planes in the domain I [35]. Similarly, after the ploughing the N(1 $\bar{1}$ 1) slip planes are also activated in the domain I, rather than the P(1 $\bar{1}$ $\bar{1}$) slip-planes (see Fig. 4(a)).

3.1.3. Pile-up morphology

Fig. 5 shows the topography after ploughing with varying lengths into the {111}, {101} and {001} grains and the corresponding maximum heights of the pile-ups with a function of ploughing length. We observe that the pile-up topographies are related closely to the corresponding slip-step patterns: 1) the front area also consists of three domains I, II and III, and the pile-up domains I and III locate two sides and no deformation occurs in the domain II; 2) during the transition from indentation to ploughing, the volume of front pile-up[2] (see an example marked with black arrows in the dashed frame in Fig. 5(a)), and the pile-up shapes grow with geometric similarity; 3) the location of the domains I and III are also similar with respect to the wear direction and the indenter center; 4) the pile-up topographies are also asymmetric on both sides of the wear track. These observations highlight that the grain orientation determines the slip-step pattern and topography. For the {111} grain orientation, higher extension and activity of slip-step in domain I shows more height in domain I, compared to those in domain II. The pile-up I locates in the front of the wear direction while the pile-up II closely to the right-hand side of imprint. For the {101} grains, the pile-up height and extension are similar in domains I and II. The height and extension of pile-up I in the {001} grains are higher than those of pile-up II, which is similar to that in the {111} grain. Fig. 5(d) illustrates that the maximum heights of the pile-ups increase until the ploughing length reaches ~10 μm, and then remain constantly in three grains, except for the right pile-up in the {111} grain.

3.2. Long ploughing

Fig. 6 shows the SEM and confocal images of 20 μm wear tracks in the {111}, {101} and {001} grains, respectively. The slip-step patterns and pile-up topographies in the wear direction are divided into four segments: indentation, transition, steady-state as well as unloading segment. The indentation segment is always the contact radius of the two bodies. Gradual changes in the slip-step patterns occur in the transition segment. The transition lengths are almost identical for all orientations, ~10 μm. This observation implies that the transition length is independent of the grain and wear track orientation. When the ploughing length exceeds ~10 μm, the slip-step patterns are stable. The length of the steady-state segment depends on the total length of the wear track. The unloading region has a length similar to the radius of the contact.

A sink-in, i.e. positive depth outside the wear track, is observed at the right-hand side of the wear track in the {110} grain and highlighted by a dashed rectangle. The data-points with a height less than zero, i.e. outside height, are highlighted with green in Fig. 6(e). A similar sink-in is observed in the {001} grain in the front of the wear track, highlighted by a blue circle. It should be pointed out that wear debris or scrapes are not observed in this study.

We further investigate the pile-up details obtained from confocal microscopy, as shown in Fig. 7. The cross-section profiles show artifacts on the banks of the wear track: there the profile is not a smooth line. These artifacts occur in confocal measurements in steep slopes and the artifacts should be ignored. Once the ploughing starts, the depth curves show that the indenter penetrates further the material and then reduces the penetration for the three grains, as shown in Fig. 7(a). A steady state is achieved after ~10 μm, which matches the transition length from slip-step pattern. The cross-section profiles in Fig. 7(b) show that the pile-up cross-section at the left-hand side in the {111} grain is much larger than that at the right-hand side; slightly larger in the {001} grain; almost same in the {101} grains. Here, it should be emphasized that the cross-section size is not only affected by the grain orientation, but also influenced by the wear direction, sample tilting effect, etc. In this study,

[2] Front pile-up is the deformed domain that locates above the sample surface and in front of the tip centerline that is perpendicular to the scratch direction.

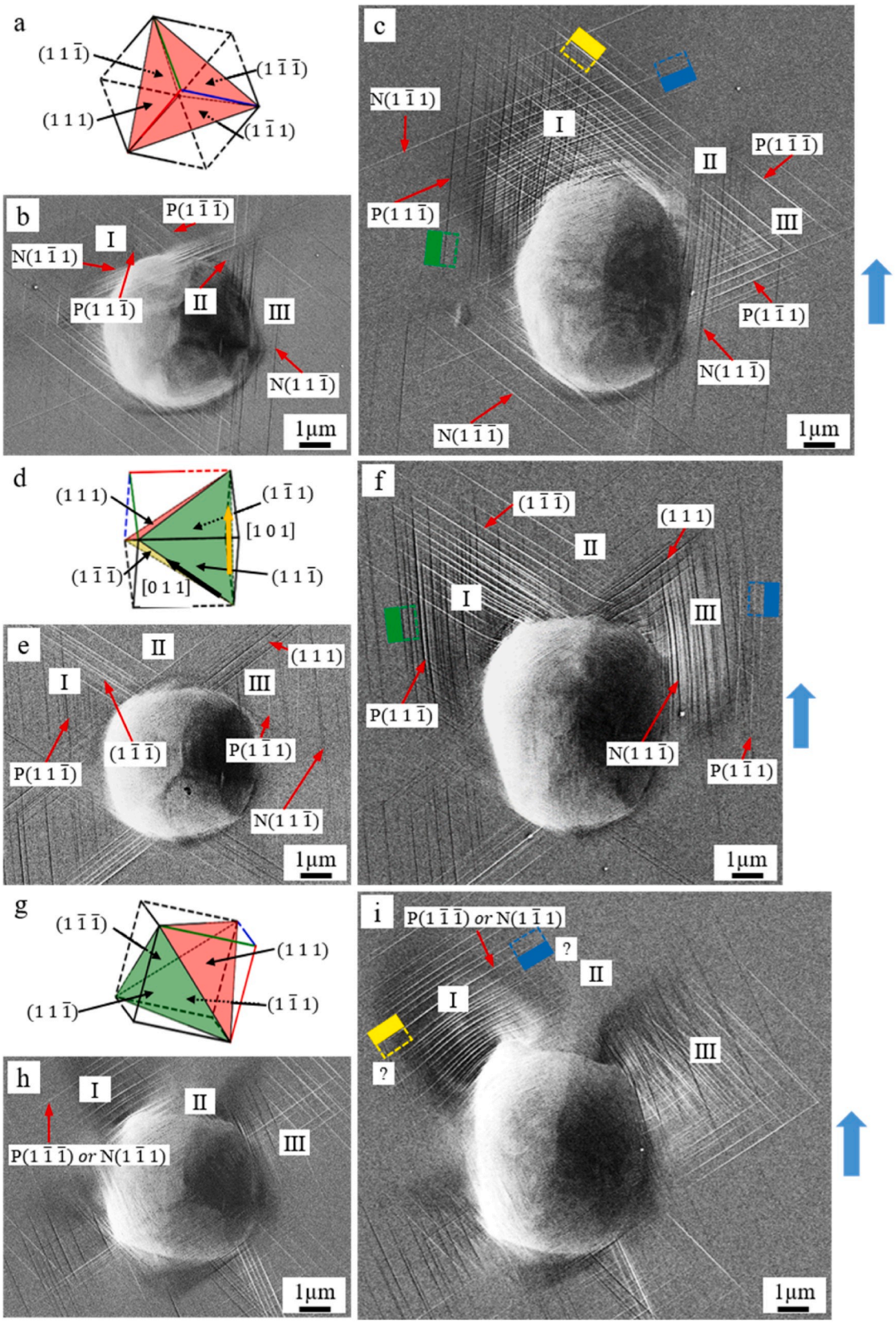

Fig. 2. SEM images after indentation and ploughing with a normal force of 40 mN and a length of 2 μm into (a)–(c) the {111} grain with the ~[1$\bar{1}$0] direction, (d)–(f) the {101} grain with the ~[011] direction and (g)–(i) the {001} grain with the ~[100] direction: (a) (d) (g) Thompson tetrahedrons; (b) (e) (h) indentation and (c) (f) (i) ploughing: P denotes for positive inclined slip planes and N negative inclined slip planes with respect to the surface; the inclination of (1 $\bar{1}$ $\bar{1}$) slip-plane is shown with the yellow frame, (1 $\bar{1}$ 1) activity blue, (1 1 $\bar{1}$) activity green and (1 1 1) activity red; Solid frame is above the surface and hollow frame with dashed lines is underneath the surface; Blue arrows indicate the wear direction; please note that the thompson tetrahedron in (a) is an inverted triangular pyramid. (For interpretation of the references to colour in this figure legend, the reader is referred to the Web version of this article.)

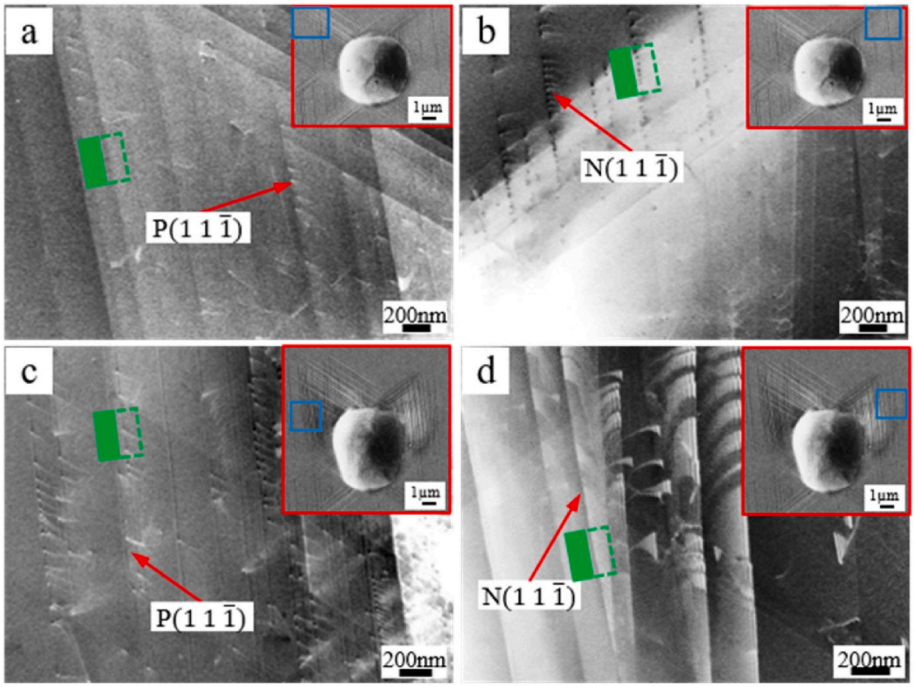

Fig. 3. ECCI images after (a) (b) indentation and (c) (d) 2 μm ploughing in the {101} grain: (a) (c) left side of imprints, i.e. domain I and (b) (d) right side of imprints, i.e. domain III: Blue frames show the corresponding precise locations of ECCI observation. (For interpretation of the references to colour in this figure legend, the reader is referred to the Web version of this article.)

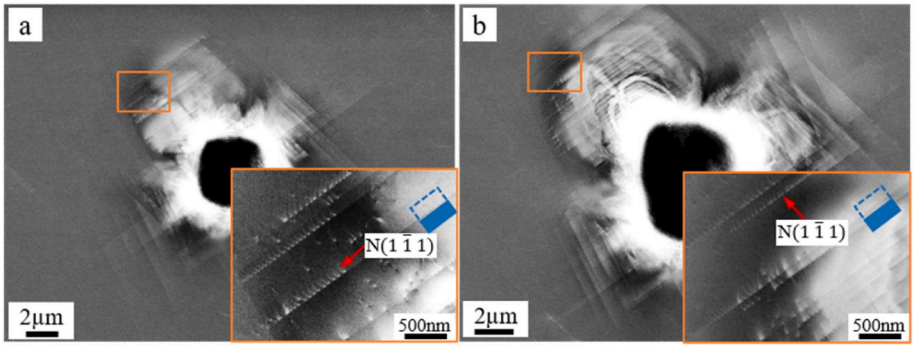

Fig. 4. ECCI images after (a) indentation and (b) 2 μm ploughing in the {001} grain.

we do not focus on the comparison among these three individual cases.

3.3. Friction force

Fig. 8 shows the development of friction force during ploughing in the {111} grain for different wear track length. This friction force evolution is not the conventional increase of friction force until the critical static friction force and the subsequent dynamic friction force. In this study, a relative motion occurs as evident by the previously shown wear tracks. Here, the friction force increases during the transition segment and reaches a steady state value. The length of the transition zone (~10 μm) is similar to the measures from the slip-step patterns and the depth. Hence, the all measures predict the same transition length. The same qualitative evolution of the friction force was observed in Refs. [9–11, 21,34].

It should be pointed out that the accuracy of the friction force measurements is limited in the nanoindenter, i.e. 2 mN. A novel approach has been developed to improve that accuracy [36]. That approach has not been used in this study, because this study focuses on the qualitative evolution of the friction force only. The friction force in the {101} and {001} grains show the same qualitative behavior and are not shown here for conciseness.

4. Discussion

4.1. 'Genetic similarity' from indentation to ploughing

The slip-step pattern and the pile-up topography are results of plastic flow. These are also complementary: the pile-up topography quantifies the plastic flow and the slip step pattern shows the slip-planes and distribution. The measures show that ploughing consists of four steps: indentation, transition, steady-state and unloading segments in the three grains. The indentation segment is the first stage of ploughing. Once the indenter starts to move laterally, it experiences a transition process and then arrives at steady-state stage. The unloading segment is the dynamic deformation area during ploughing.

The dominant slip planes in the indentation segment remain active in the subsequent ploughing segment. During ploughing the activated slip-planes and pile-up in the unloading segment shift parallel, i.e. same relative location of domains I and III, with respective to the indenter

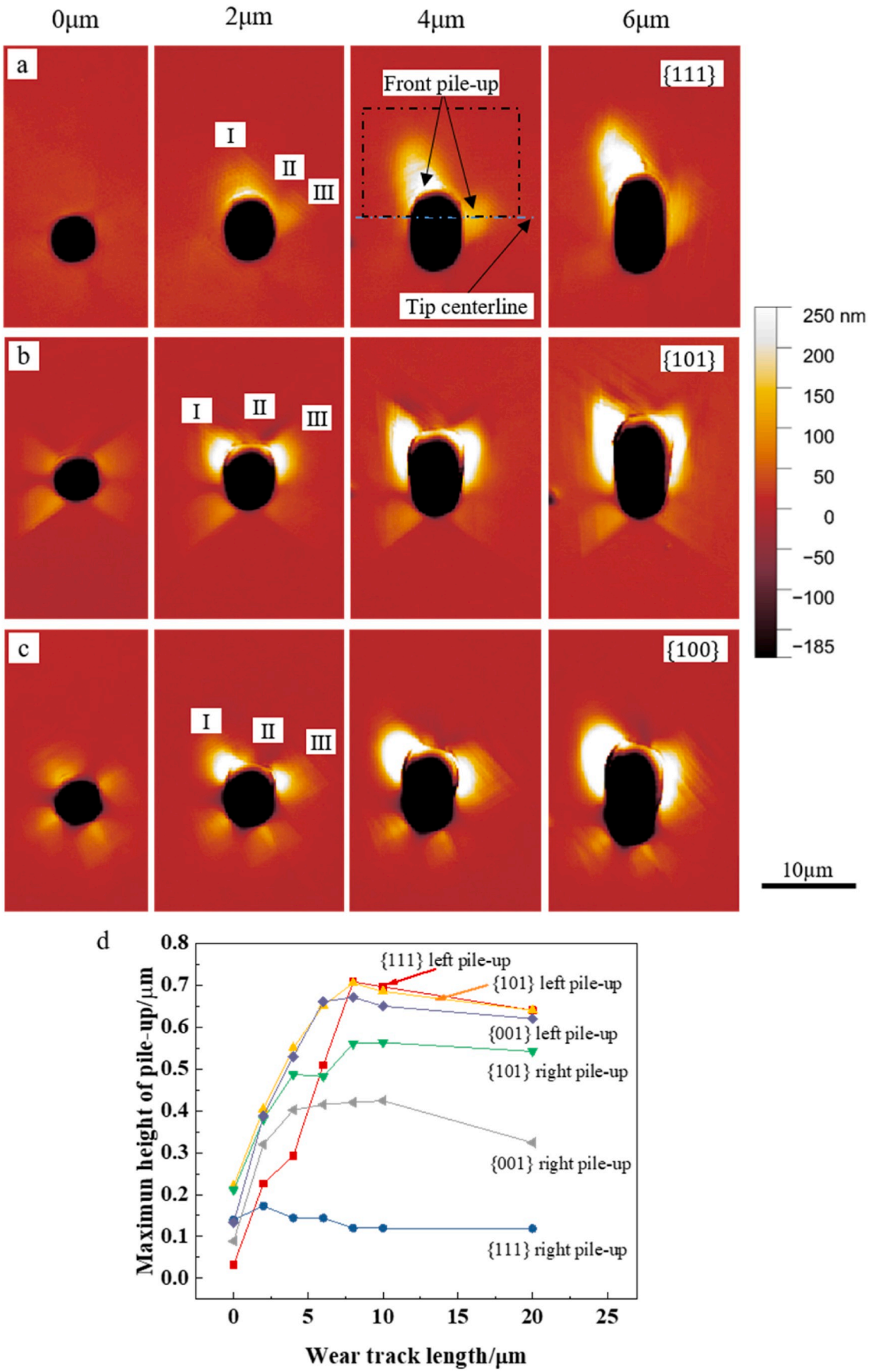

Fig. 5. Topographies after indenting and ploughing with different ploughing lengths into the (a) {111} grain, (b) {101} grain and (c) {001} grain. (d) shows the maximum heights of pile-ups as a function of wear track length.

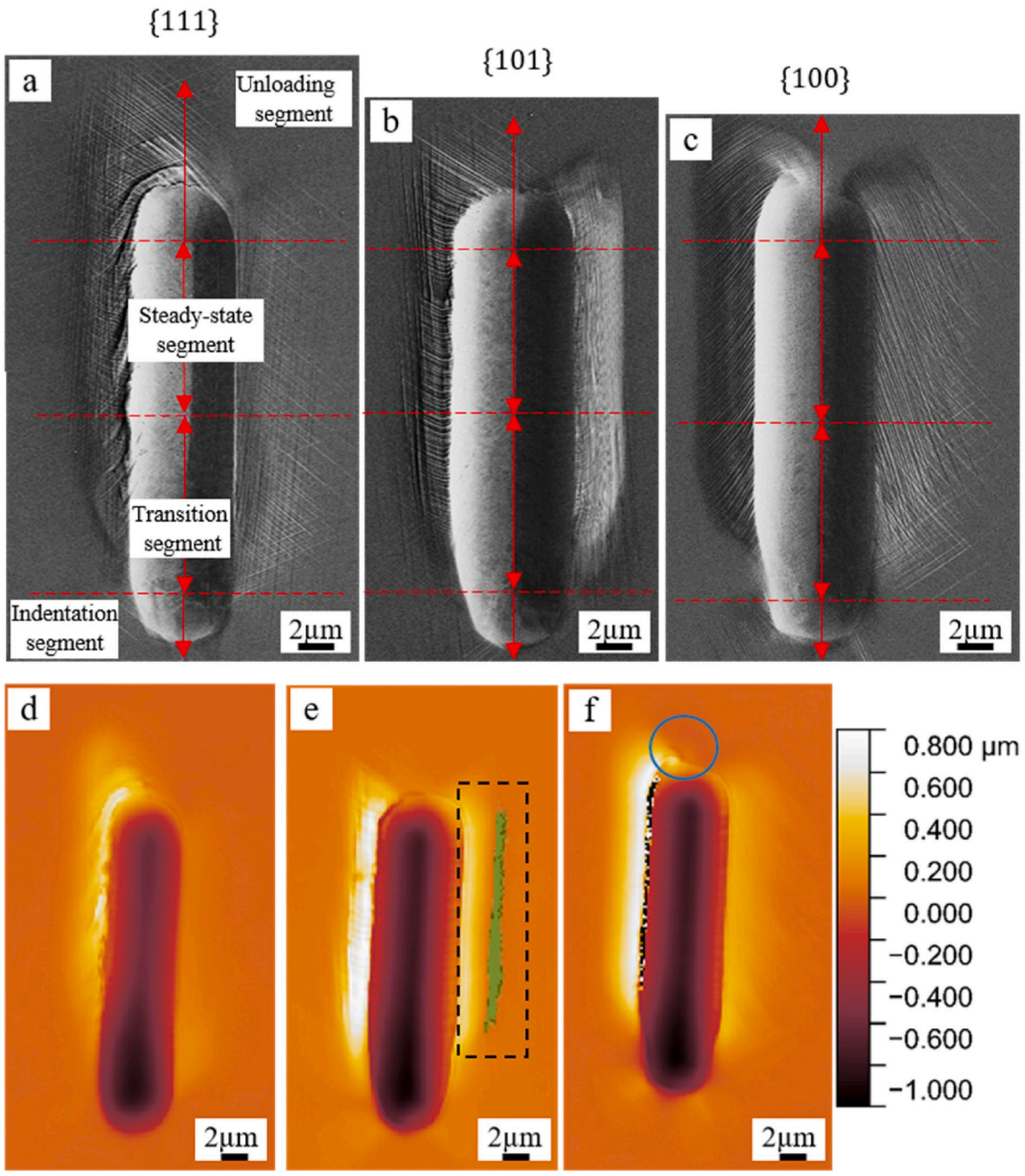

Fig. 6. (a)- (c) SEM and (d)- (f) confocal images of the wear tracks with a length of 20 μm. In the (a) (d) {111}[1$\bar{1}$0] grain, (b) (e) {101}[011] grain and (c) (f) {001}[100] grain, which denotes the normal and wear direction.

center and the wear direction, and the intensity increases. Here, we address the absence of additional slip systems during ploughing at the example of the {1 0 0} grain. During indentation, the primary P(1 1 1) and P(1 1 $\bar{1}$) slip systems produce a pile-up and result in the activation of the N(1 $\bar{1}$ 1) slip system [35].[3] Once the indenter starts the ploughing, the P(1 $\bar{1}$ $\bar{1}$) plane is a favorable slip system in domain II, compared to the N(1 $\bar{1}$ 1) plane. However, as shown by ECCI in Fig. 4 (b), slip on the N(1 $\bar{1}$ 1) slip-planes dominate, rather than on the P(1 $\bar{1}$ $\bar{1}$) plane, because (i) this plane is negatively inclined allowing efficient plasticity once the pile-up is established and (ii) pre-existing dislocations exist on these N(1 $\bar{1}$ 1) planes. The same observations are applicable to domain I of the {1 1 1} grain. Further CP-FEM or DDD simulations are required to investigate the stress fields during the transition from indentation to ploughing.

4.2. *Differences between indentation and ploughing*

Ploughing consists of two phases, indentation and lateral motion. Because the lateral motion phase breaks the indentation symmetry, differences in plasticity between indentation and ploughing are expected. Moreover, during ploughing, the depth increases initially and

[3] Slip on the (1 1 1) slip-plane, which is parallel to the surface cannot be observed. Hence, this slip-plane is not discussed here. Note that the resolved shear stress is close to 0 on this plane.

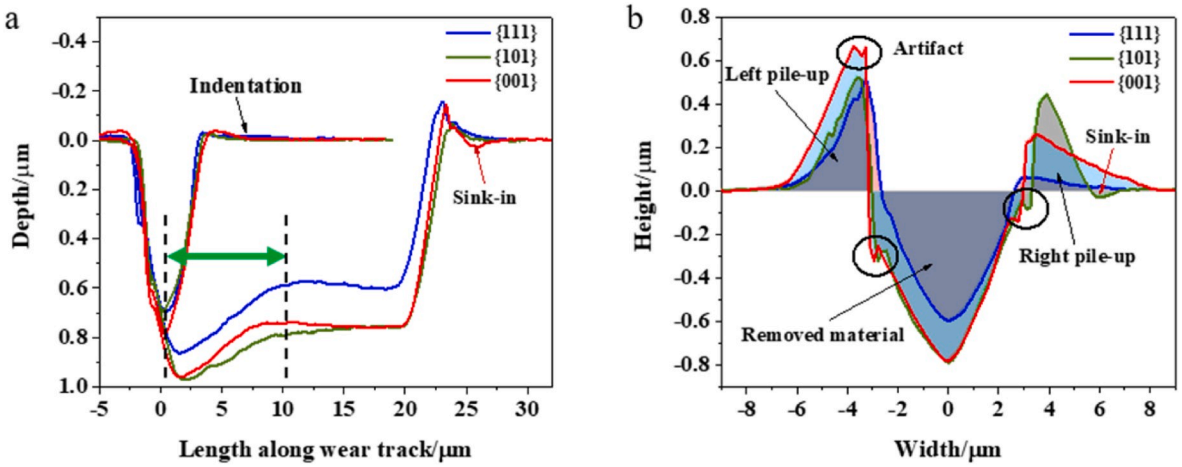

Fig. 7. Corresponding cross-sectional profiles in 20 μm wear tracks in the {111}, {101} and {001} grains: (a) shows the depth along the central line of the wear track and (b) illustrates the cross-section profile in the steady-state segment.

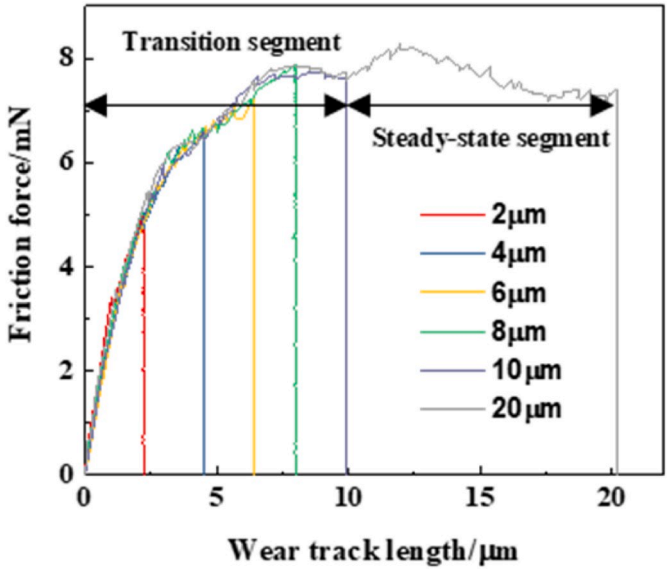

Fig. 8. Friction force as a function of wear track length in the {111} grain. The behavior of the other grain orientations is similar.

then decreases towards the steady-state depth, which also inevitably results in the differences from the indentation to the ploughing.

One different is that slip sequence change for some cases. During ploughing, the negatively inclined N(1 1 $\bar{1}$) slip-planes are dominant on the sides of the wear track in the domains III of the {1 1 1} and {1 0 1} grains (see Fig. 2). However, they are both secondary slip systems during indentation [35]. Gagel et al. [25] and Greiner et al. [4] demonstrated how dislocations move into initially dislocation free regions during sliding and the authors discussed how sliding direction, the orientations of glide plane and Burgers vector affect dislocation motion. In this study, the pre-existing dislocations on these N(1 1 $\bar{1}$) slip-planes from the indentation segment also move along the wear direction and – moreover – these dislocations multiplied. Hence, the slip-planes with transportable dislocations during the indentation segment can be primary slip systems during the ploughing. The slip-step pattern on these N(1 1 $\bar{1}$) slip-planes becomes wider because the plasticity continuous to spread away, due to the lateral motion phase together with the increased stress components induced by indentation phase, not caused by dislocation transport.

Another difference is the dislocation behavior. Only perfect dislocations are observed after indentation in the {101} grain in this study (even using 80 mN normal force in Ref. [35]). It means that the dislocations cannot be dissociated into partial dislocations in the indentation phase during ploughing. However, after ploughing, dissociated dislocations occur on the one-side of the wear track. Hence, these dissociated dislocations on the negatively inclined right-hand (1 1 $\bar{1}$) planes are mainly caused by the lateral stress. On these negatively inclined planes, the most possible Burgers vector is $a/2$[1 0 1] (see the yellow arrow in Fig. 2(d)), which leading to the dislocation transport and more plasticity towards the front side on this principle slip system. Due to the effect of the lateral stress, the corresponding leading partial dislocation is expected to have a higher Schmid factor than the trailing partial dislocation, hence the perfect dislocations with a Burgers vector of $a/2$[1 0 1] are dissociated into the partial dislocations. Moreover, on the left-hand side of the wear track, the dislocations in the P(1 1 $\bar{1}$) planes are still perfect, because the Burgers vector on these planes most likely is $a/2$[0 1 1] (see the black arrow in Fig. 2(d)), which results in plasticity spread more easily away from the indenter, while the Schmid factor of the corresponding leading partial dislocation is expected to be lower than that of the trailing partial dislocation.

4.3. Slip-step and pile-up evolutions

The slip-step and pile-up evolutions are the grain orientation dependence. It should be noted here that the wear direction also influences the plasticity, however, this is not the focus of this work. The indentation is the first stage of the ploughing process, which provides numerous 'pre-existing' dislocations for the following ploughing process. The indentation-induced plasticity has been revealed in Ref. [35, 37]. The dislocations nucleate underneath the indenter and travel on the positively inclined slip-planes during the initial stage of indentation, resulting in the formations of pile-ups. The tilting angle of the slip-planes determine the plasticity flow directions in the planes. Afterwards, the pile-up formation is contributed to the slip on the negatively inclined slip-plane. In order to better discuss, the indentation imprint is also divided into two segments: indentation at the backside of indenter and unloading segment at the front side. Here, we mainly focus on the unloading segment, as it is a dynamic deformation domain during the ploughing.

Once the indenter starts to wear, it penetrates further and then moves back. When it ploughs beyond a length of ~10 μm, the depth remains constant for all three grain orientations. This depth development matches the evolutions of the slip-step pattern and pile-up topography: transition and steady-state segments, respectively. These critical lengths are independent of the grain orientation.

In the {111} grain, two pile-ups and corresponding slip-steps form at the unloading segments during indentation (see Figs. 2 and 5). In the domain I, slip on the P(1 1 $\bar{1}$) and P(1 $\bar{1}$ $\bar{1}$) planes determine the initial site of the pile-up, which is closer to the front of indenter during indentation. During ploughing, the additional lateral stress leads to a larger deformation while the center location of this domain almost does not rotate with respect to the wear direction and the indenter center. The N(1 $\bar{1}$ 1) slip-plane in this domain is still the secondary slip system. The site of the domain III during indentation is mainly determined by slip on the P(1 $\bar{1}$ 1) and P(1 $\bar{1}$ $\bar{1}$) planes. It locates close to the clockwise direction of ~80°, far away from the front of the indenter, which leads to a slight influence from the lateral stress. The N(1 1 $\bar{1}$) slip planes become a principle slip system and the dislocations on these planes are transported and multiplied with the indenter due to the plough component, which result in a forward flow of plasticity, as we can see from the growth of the corresponding slip-steps in Fig. 2(c). The transported dislocations are not only from the pre-existing dislocations that were produced in the indentation segment, but also induced by the following increased wear depth effect and lateral stress.

In the {101} grain, the pile-ups at the two sides of the imprints grow with symmetry relationships during ploughing, because the grain orientation is close to the ideal {101} and the wear direction is near to the [011] symmetry axis. However, due to the small deviation from the ideal {101} and the symmetry axis, some differences between the domains I and III are inevitable. One difference is that the width and height of the left pile-up are slightly larger than that at the right-hand side (see Fig. 7), most possibly because the plasticity flows on the P(1 1 $\bar{1}$) plane towards the front-left side with the presence of Burgers vector $a/2$[0 1 1] (see Fig. 2(d)). The N(1 1 $\bar{1}$) plane at the right side becomes a principle slip system during ploughing, leading to more plasticity towards the front side with presence of Burgers vector $a/2$[1 0 1] (dissociated into two partials). Moreover, the neutral (1 1 1) slip-planes are activated in the domain I close to the imprint during indentation. After ploughing, it plays a barrier in the plasticity flow to the front-left side and promotes the plasticity flowing upwards in the domain I and close to the imprint, which results in slight higher height in the domain I than in the domain III. The second difference is that only sink-in is found at the right side of domain III in which have numerous negatively inclined slip system. The sink-in is a normal phenomenon for some materials during indentations, which locates close to the indenter [38,39]. Kim et al. [40] reported that the sink-in can occur at the opposite side of pile-up with respect to the indenter and claimed that it is caused by elastic deflection during indentation. Here, it is possibly induced by material flow on the main slip system N(1 1 $\bar{1}$) planes in this domain. Further CP-FEM or other simulations are required to unravel the mechanism of sink-in.

4.4. Friction force evolution

In this subsection, we focus on the friction force development. The apparent friction force F_{fric} is decomposed into an adhesive friction F_{ad} and ploughing friction F_{pl} [18]. Based on it, Lafaye et al. [16–18] proposed the analytical models with the consideration of elastic recovery, which show that the tendencies of friction and depth should be similar, i.e. positive relationship. However, the results in this study show that the friction increases significantly first and then slightly till to it stays flat while the depth increases and then decreases until to reach the steady state (see Fig. 7). Therefore, the change in wear depth is not main reason accounting for the development of friction force. Fig. 5 shows that the pile-up in the front of indenter has a similar tendency to the friction development. Pile-up increase results in an increase in the ploughing friction, F_{pl} and – finally – friction force increase. Therefore, pile-up is a dominant factor for the friction increase, rather than the depth change.

5. Conclusion

Based on the investigation of the evolution of plasticity and friction in three grains in an austenite stainless steel, the following conclusions can be drawn:

1. The plastic flow during ploughing, i.e. slip-step and pile-up evolutions, has four stages: indentation, transition, steady-state as well as unloading segments. The transition lengths are ~10 μm in these grains.
2. The indentation stage affects the following stages. During the transition, the center of slip-step pattern and pile-up tend to remain in the same direction with respect to the wear direction. Moreover, the active slip systems remain constantly during the deformation.
3. Differences exist between indentation and ploughing due to the lateral motion and due to the change in wear depth:
   a. The symmetry of the pile-up is broken by the wear motion
   b. The relative activity of slip systems change depending on the grain orientation.
   c. Dissociated dislocations occur during wear while indentation is dominated by full dislocations.
4. The friction force starts from 0 N and increases until it reaches a steady-state value when exceeding a length of ~10 μm, independent of the studied grain orientations. The increase in friction force and the steady state force are caused by the increase of the pile-up in front of the asperity.

Declaration of competing interest

We wish to confirm that there are no known conflicts of interest associated with this publication.

CRediT authorship contribution statement

Wenzhen Xia: Conceptualization, Methodology, Data curation, Formal analysis, Writing - original draft. **Gerhard Dehm:** Supervision, Writing - review & editing. **Steffen Brinckmann:** Project administration, Conceptualization, Formal analysis, Supervision, Writing - review & editing.

Acknowledgments

The authors appreciate the funding of the Deutsche Forschungsgemeinschaft (DFG)−project No.: BR-3947/5–1.

Appendix A. Supplementary data

Supplementary data to this article can be found online at https://doi.org/10.1016/j.wear.2020.203289.

References

[1] B. Bhushan, Introduction to Tribology, John Wiley & Sons, 2013.
[2] I. Hutchings, P.H. Shipway, Tribology: Friction and Wear of Engineering Materials, Butterworth-Heinemann, 2017.
[3] B. Bhushan, Nanotribology and nanomechanics: an introduction, Tribol. Lubric. Technol. 73 (9) (2017), 78-78, fourth ed.
[4] C. Greiner, J. Gagel, P. Gumbsch, Solids under extreme shear: friction-mediated subsurface structural transformations, Adv. Mater. 31 (26) (2019).
[5] X. Chen, R. Schneider, P. Gumbsch, C. Greiner, Microstructure evolution and deformation mechanisms during high rate and cryogenic sliding of copper, Acta Mater. 161 (2018) 138–149.
[6] D. Tabor, The physical meaning of indentation and scratch hardness, Br. J. Appl. Phys. 7 (5) (1956) 159–166.
[7] J.A. Williams, Analytical models of scratch hardness, Tribol. Int. 29 (8) (1996) 675–694.
[8] V. Jardret, H. Zahouani, J.L. Loubet, T.G. Mathia, Understanding and quantification of elastic and plastic deformation during a scratch test, Wear 218 (1) (1998) 8–14.

[9] S. Brinckmann, C.A.C. Fink, G. Dehm, Nanotribology in austenite: normal force dependence, Wear 338 (2015) 430–435.
[10] S. Brinckmann, G. Dehm, Nanotribology in austenite: plastic plowing and crack formation, Wear 338 (2015) 436–440.
[11] H.R. Chamani, M.R. Ayatollahi, The effect of Berkovich tip orientations on friction coefficient in nanoscratch testing of metals, Tribol. Int. 103 (2016) 25–36.
[12] C. Li, F.H. Zhang, B.B. Meng, X.S. Rao, Y. Zhou, Research of material removal and deformation mechanism for single crystal GGG (Gd3Ga5O12) based on varied-depth nanoscratch testing, Mater. Des. 125 (2017) 180–188.
[13] R.W. Carpick, Scratching the Surface: fundamental investigations of tribology with atomic force microscopy, Chem. Rev. 97 (4) (1997) 1163–1194.
[14] F.P. Bowden, D. Tabor, The Friction and Lubrification of Solids, vol. 1, Clarendon Press, Oxford, 1950–1954.
[15] D.F. Moore, The Friction and Lubrication of Elastomers, Pergamon Press, London, 1972.
[16] S. Lafaye, C. Gauthier, R. Schirrer, The ploughing friction: analytical model with elastic recovery for a conical tip with a blunted spherical extremity, Tribol. Lett. 21 (2) (2006) 95–99.
[17] S. Lafaye, C. Gauthier, R. Schirrer, Analysis of the apparent friction of polymeric surfaces, J. Mater. Sci. 41 (19) (2006) 6441–6452.
[18] S. Lafaye, M. Troyon, On the friction behaviour in nanoscratch testing, Wear 261 (7–8) (2006) 905–913.
[19] J. Goddard, H. Wilman, A theory of friction and wear during the abrasion of metals, Wear 5 (1962) 114–135.
[20] J.Y. Huang, F.A. Ponce, P.G. Caldas, R. Prioli, C.M. Almeida, The effect of nanoscratching direction on the plastic deformation and surface morphology of InP crystals, J. Appl. Phys. 114 (20) (2013).
[21] Z.F. Wang, H.J. Zhang, Z.Q. Li, G. Li, J.J. Zhang, J.G. Zhang, H. ul Hassan, Y. D. Yan, A. Hartmaier, T. Sun, Crystal plasticity finite element simulation and experiment investigation of nanoscratching of single crystalline copper, Wear 430 (2019) 100–107.
[22] N. Duan, Y.Q. Yu, W.S. Wang, X.P. Xu, Analysis of grit interference mechanisms for the double scratching of monocrystalline silicon carbide by coupling the FEM and SPH, Int. J. Mach. Tool Manufact. 120 (2017) 49–60.
[23] Z. Guo, Y. Tian, X. Liu, F. Wang, C. Zhou, D. Zhang, Modeling and simulation of the probe tip based nanochannel scratching, Precis. Eng. 49 (2017) 136–145.
[24] F. Roters, P. Eisenlohr, C. Kords, D.D. Tjahjanto, M. Diehl, D. Raabe, DAMASK: the Dusseldorf Advanced MAterial Simulation Kit for studying crystal plasticity using an FE based or a spectral numerical solver, Proc Iutam 3 (2012) 3–10.
[25] J. Gagel, D. Weygand, P. Gumbsch, Discrete Dislocation Dynamics simulations of dislocation transport during sliding, Acta Mater. 156 (2018) 215–227.
[26] D. Mulliah, S.D. Kenny, R. Smith, C.F. Sanz-Navarro, Molecular dynamic simulations of nanoscratching of silver(100), Nanotechnology 15 (3) (2004) 243–249.
[27] T. Junge, J.F. Molinari, Plastic activity in nanoscratch molecular dynamics simulations of pure aluminium, Int. J. Plast. 53 (2014) 90–106.
[28] S. Jun, Y. Lee, S.Y. Kim, S. Im, Large-scale molecular dynamics simulations of Al (111) nanoscratching, Nanotechnology 15 (9) (2004) 1169–1174.
[29] P.Z. Zhu, Y.Z. Hu, F.Z. Fang, H. Wang, Multiscale simulations of nanoindentation and nanoscratch of single crystal copper, Appl. Surf. Sci. 258 (10) (2012) 4624–4631.
[30] J. Li, B. Liu, H. Luo, Q.H. Fang, Y.W. Liu, Y. Liu, A molecular dynamics investigation into plastic deformation mechanism of nanocrystalline copper for different nanoscratching rates, Comput. Mater. Sci. 118 (2016) 66–76.
[31] J.C. Huang, Evaluation of tribological behavior of Al-Co-Cr-Fe-Ni high entropy alloy using molecular dynamics simulation, Scanning 34 (5) (2012) 325–331.
[32] Z.N. Wang, J. Li, Q.H. Fang, B. Liu, L.C. Zhang, Investigation into nanoscratching mechanical response of AlCrCuFeNi high-entropy alloys using atomic simulations, Appl. Surf. Sci. 416 (2017) 470–481.
[33] Y.X. Ye, C.Z. Liu, H. Wang, T.G. Nieh, Friction and wear behavior of a single-phase equiatomic TiZrHfNb high-entropy alloy studied using a nanoscratch technique, Acta Mater. 147 (2018) 78–89.
[34] Y. Zhang, L.C. Zhang, M. Liu, F.H. Zhang, K. Mylvaganam, W.D. Liu, Understanding the friction and wear of KDP crystals by nanoscratching, Wear 332 (2015) 900–906.
[35] W. Xia, G. Dehm, S. Brinckmann, Unraveling indentation-induced slip steps in austenitic stainless steel, Mater. Des. 183 (2019) 108169.
[36] S. Brinckmann, R. Soler, G. Dehm, Towards quantifying the shear delamination of thin films, Materialia 8 (2019).
[37] W. Xia, G. Dehm, S. Brinckmann, Insight into Indentation-Induced Plastic Flow in Austenitic Stainless Steel, J. Mater. Sci., 2020, https://doi.org/10.1007/s10853-020-04646-y. In press.
[38] V. Karthik, P. Visweswaran, A. Bhushan, D.N. Pawaskar, K.V. Kasiviswanathan, T. Jayakumar, B. Raj, Finite element analysis of spherical indentation to study pile-up/sink-in phenomena in steels and experimental validation, Int. J. Mech. Sci. 54 (1) (2012) 74–83.
[39] J. Rodriguez, M.A.G. Maneiro, A procedure to prevent pile up effects on the analysis of spherical indentation data in elastic-plastic materials, Mech. Mater. 39 (11) (2007) 987–997.
[40] S.H. Kim, B.W. Lee, Y. Choi, D. Kwon, Quantitative determination of contact depth during spherical indentation of metallic materials - a FEM study, Mat Sci Eng a-Struct 415 (1–2) (2006) 59–65.